

Periods and damping rates of fast sausage oscillations in multi-shelled coronal loops

Shao-Xia Chen¹ · Bo Li¹ · Li-Dong Xia¹ ·
Hui Yu¹

© Springer ●●●

Abstract Standing sausage modes are important in interpreting quasi-periodic pulsations in the lightcurves of solar flares. Their periods and damping times play an important role in seismologically diagnosing key parameters like the magnetic field strength in regions where flare energy is released. Usually such applications are based on theoretical results neglecting unresolved fine structures in magnetized loops. However, the existence of fine structuring is suggested on both theoretical and observational grounds. Adopting the framework of cold magnetohydrodynamics (MHD), we model coronal loops as magnetized cylinders with a transverse equilibrium density profile comprising a monolithic part and a modulation due to fine structuring in the form of concentric shells. The equation governing the transverse velocity perturbation is solved with an initial-value-problem approach, and the effects of fine structuring on the periods P and damping times τ of global, leaky, standing sausage modes are examined. A parameter study shows that fine structuring, be it periodically or randomly distributed, brings changes of only a few percent to P and τ when there are more than about ten shells. The monolithic part, its steepness in particular, plays a far more important role in determining P and τ . We conclude that when measured values of P and τ of sausage modes are used for seismological purposes, it is justified to use theoretical results where the effects due to fine structuring are neglected.

Keywords: Coronal Seismology; Magnetic fields, Corona; Waves, Magnetohydrodynamic

✉ Bo Li
bbl@sdu.edu.cn

¹ Shandong Provincial Key Laboratory of Optical Astronomy and Solar-Terrestrial Environment, and Institute of Space Sciences, Shandong University Weihai, Weihai 264209, China

1. Introduction

Low-frequency magnetohydrodynamic (MHD) waves and oscillations have been abundantly detected in the solar atmosphere with both spectroscopic and imaging instruments since the late 1990s with the advent of the TRACE, SOHO and *Hinode* satellites. This has led to the rapid development of coronal seismology, enabling the inference of atmospheric parameters difficult to measure directly (for recent reviews, see *e.g.*, Nakariakov and Verwichte, 2005; Stepanov, Zaitsev, and Nakariakov, 2012). To name but a few, seismological applications can offer such key information as the magnetic field strength in coronal loops (*e.g.*, Nakariakov and Ofman, 2001) and above streamer stalks (Chen *et al.*, 2010, 2011), the magnitude of field-aligned loop flows (Li, Habbal, and Chen, 2013; Chen *et al.*, 2014), as well as how the density is distributed transverse to coronal loops (Arregui *et al.*, 2007; Goossens *et al.*, 2008).

In the context of coronal seismology, sausage waves were examined primarily in connection to their potential for interpreting second-scale quasi-periodic pulsations (QPPs) in flare lightcurves (see the review by Nakariakov and Melnikov, 2009). Two regimes of sausage waves are known to exist, depending on the wavenumber k in the direction of magnetic structures hosting them (*e.g.*, Roberts, Edwin, and Benz, 1984). When k exceeds some critical k_c , the trapped regime results, whereby the wave energy is well confined to magnetic structures. If on the contrary, $k < k_c$, the leaky regime results, and sausage waves experience apparent damping by emitting waves into the surrounding fluids. For standing sausage modes, it is now well established that their period P increases steadily with decreasing k until saturating when k is sufficiently small. Identically infinite in the trapped regime for ideal MHD fluids, the damping time τ decreases with decreasing k until a saturation value is reached for sufficiently small k (*e.g.*, Kopylova *et al.*, 2007; Nakariakov, Hornsey, and Melnikov, 2012; Vasheghani Farahani *et al.*, 2014).

Both the period P and damping time τ of sausage modes are important from the seismological perspective due to their dependence on the atmospheric parameters. Let a and L denote the half-width and length of a coronal structure, respectively. In addition, let v_{Ai} (v_{Ae}) be the internal (external) Alfvén speed. For trapped modes, it is well known that the period P is determined by L/v_{ph} with the phase speed v_{ph} lying in the range between v_{Ai} and v_{Ae} (*e.g.*, Aschwanden, Nakariakov, and Melnikov, 2004). On the other hand, for leaky modes the period P was found to depend primarily on the internal Alfvén transit time a/v_{Ai} , while the ratio τ/P is primarily determined by the density contrast ρ_i/ρ_e between the structure and its surroundings (*e.g.*, Kopylova *et al.*, 2007). For both P and τ , the detailed form, the steepness in particular, of the transverse density distribution can play a subtle role (Nakariakov, Hornsey, and Melnikov, 2012; Hornsey, Nakariakov, and Fludra, 2014). Regarding the applications of measurements of leaky sausage modes, inferring a/v_{Ai} is important given the importance for inferring the coronal magnetic field strength. The inference of ρ_i/ρ_e and density profile steepness, on the other hand, is also important because these two parameters are key to determining the efficiency of such coronal heating

mechanisms as phase-mixing (Heyvaerts and Priest, 1983) and resonant absorption (see the review by Goossens, Erdélyi, and Ruderman, 2011, and references therein).

The current conclusions on the behavior of P and τ of sausage modes are mainly based on theoretical and modeling efforts where the density structuring transverse to oscillating loops is either in a piecewise-constant (tophat) form (*e.g.*, Roberts, Edwin, and Benz, 1984; Kopylova *et al.*, 2007) or described by some smooth functions (*e.g.*, Nakariakov, Hornsey, and Melnikov, 2012). However, both theoretical and observational studies indicate that coronal loops may not be regularly structured but contain unresolved, fine structuring. For instance, density measurements (Tripathi *et al.*, 2009; Brooks, Warren, and Ugarte-Urra, 2012), and temperature diagnostics (*e.g.*, Warren *et al.*, 2008; Brooks *et al.*, 2013) suggest that loops with apparent widths $\gtrsim 1000$ km are likely to comprise a multitude of fine structures, the scales of which may be down to $\lesssim 15$ km (Peter *et al.*, 2013). On the theoretical side, numerical simulations on the temporal evolution of coronal loops (*e.g.*, Reale and Peres, 2000; Warren, Winebarger, and Mariska, 2003; Guarrasi, Reale, and Peres, 2010) indicate the need to invoke threads with widths ~ 100 km to better reproduce direct observables. Interestingly, further evidence showing the existence of fine structuring is found from a seismological standpoint by Van Doorselaere *et al.* (2008) when interpreting the CoMP measurements of propagating transverse waves. The increasing consensus on the existence of fine structuring in coronal structures has also stimulated the interest in examining the influence of fine structuring on coronal seismology (*e.g.*, Murawski, Nakariakov, and Pelinovsky, 2001; Pascoe, Nakariakov, and Arber, 2007; Yuan *et al.*, 2015). Regarding sausage modes, the study by Pascoe, Nakariakov, and Arber (2007, hereafter PNA07) is of particular relevance since it focuses on how fine structuring influences the period P of trapped modes. Modeling coronal loops as a magnetic slab with either periodical or random fine structuring, PNA07 find that P of fundamental trapped modes is insensitive to fine structuring.

While the study by PNA07 is reassuring for seismological applications based on measured values of sausage periods, it is natural to ask: Does this conclusion hold also for magnetic cylinders? In addition, what will be the influence of fine structuring on the leaky modes, the damping time τ in particular? These questions are addressed in the present study. This manuscript is organized as follows. In Section 2 we present the necessary equations and our method of solution. A parameter study is then presented in Section 3 to examine in detail the changes to P and τ due to fine structuring relative to the case where fine structuring is absent. Section 4 closes this manuscript with our summary and some concluding remarks.

2. Model Description and Method of Solution

We work in the framework of cold (zero-beta) MHD, appropriate for the solar corona, and model coronal loops as straight cylinders whose axes coincide with the z -axis in a cylindrical coordinate system (r, θ, z) . The equilibrium magnetic

field $\bar{\mathbf{B}}$ is uniform and also in the z -direction ($\bar{\mathbf{B}} = \bar{B}\hat{z}$). The equilibrium density $\bar{\rho}$ is assumed to be a function of r only. In this regard, the modeled fine structures are concentric shells sharing the same axis as the cylinder. Considering only fundamental standing sausage modes supported by loops of length L , we can express the radial component of the perturbed velocity as $\delta v_r(r, z, t) = v(r, t) \sin(kz)$ with the axial wavenumber k being π/L . It then follows from linearized, ideal, cold MHD equations that (see Nakariakov, Hornsey, and Melnikov, 2012)

$$\frac{\partial^2 v(r, t)}{\partial t^2} = v_A^2(r) \left[\frac{\partial^2}{\partial r^2} + \frac{1}{r} \frac{\partial}{\partial r} - \left(k^2 + \frac{1}{r^2} \right) \right] v(r, t), \quad (1)$$

where $v_A(r) = \bar{B}/\sqrt{4\pi\bar{\rho}(r)}$ is the Alfvén speed. The boundary conditions appropriate for sausage modes are

$$v(r, t)|_{r=0} = 0, \quad v(r, t)|_{r \rightarrow \infty} = 0. \quad (2)$$

Furthermore, the following initial conditions (ICs)

$$v(r, t)|_{t=0} = \frac{r}{1+r^2}, \quad \left. \frac{\partial v(r, t)}{\partial t} \right|_{t=0} = 0 \quad (3)$$

are adopted. While in principle the ICs can be arbitrary, the form given in Equation (3) ensures that only waves with the simplest radial structure are primarily excited.

Similar to PNA07, the equilibrium density $\bar{\rho}(r)$ consists of two parts, a background monolithic one (ρ_{mono}) modulated by a distribution due to fine structuring (ρ_{FS}). In other words,

$$\bar{\rho}(r) = \rho_{\text{mono}}(r) + \rho_{\text{FS}}(r), \quad (4)$$

$$\rho_{\text{mono}}(r) = \rho_e + (\rho_i - \rho_e) f(r), \quad (5)$$

$$\rho_{\text{FS}}(r) = (\rho_i - \rho_e) g(r) f(r). \quad (6)$$

The function $f(r)$ decreases smoothly from unity at the cylinder axis ($r = 0$) to zero at infinity, ensuring that $\rho_{\text{mono}}(r)$ decreases smoothly from ρ_i at $r = 0$ to ρ_e at infinity. On the other hand, $g(r)$, which describes the fine structures in the form of concentric shells, cannot exceed unity to avoid negative values of $\bar{\rho}$. To maximize the effects due to fine structuring, we set the maximum of $g(r)$ to be unity.

With the boundary (Equation (2)) and initial (Equation (3)) conditions, Equation (1) can be evolved once $f(r)$ and $g(r)$ are specified. In practice, we solve Equation (1) with a finite-difference (FD) scheme second-order accurate in both time and space. To save computational time, a non-uniform computational grid $\{r_i, i = 1, 2, \dots, I\}$ is adopted with $r_1 = 0$ and $r_I = 1000a$, where a is the cylinder radius. The grid spacing $\{\Delta r_i = r_{i+1} - r_i, i = 1, 2, \dots, I - 1\}$ is identically $0.001a$ for $r \leq 4a$. Then Δr_i increases in the manner $\Delta r_{i+1} = 1.025\Delta r_i$ until Δr_i reaches $\sqrt{\rho_i/\rho_e} \times \Delta r_1$. From there on Δr_i remains uniform again. To ensure numerical stability, a uniform timestep $\Delta t = 0.8\Delta r_{\text{min}}/v_{A,\text{max}}$ is set according to the Courant condition, where $\Delta r_{\text{min}}(v_{A,\text{max}})$ denotes the minimal

(maximal) value of $\{\Delta r_i\}$ ($\{v_{A,i} = \bar{B}/\sqrt{4\pi\bar{\rho}(r_i)}\}$). In response to the initial condition (Equation (3)), disturbances are generated and propagate away from the cylinder. However, as shown in Nakariakov, Hornsey, and Melnikov (2012), two regimes can be readily distinguished if one follows the temporal evolution of the perturbation at, say, $r = a$. For $k = \pi/L$ larger (smaller) than some critical value, this $v(a, t)$ evolves into a harmonic (decaying harmonic) form, corresponding to the well-known trapped (leaky) regime. Numerically fitting $v(a, t)$ with a sinusoidal (exponentially decaying sinusoidal) function then yields the period P (P together with the damping time τ) for trapped (leaky) modes. It suffices to note here that P and τ depend only on the combination $[f(r), g(r); L/a, \rho_i/\rho_e]$ when P and τ are measured in units of the internal Alfvén transit time a/v_{Ai} with v_{Ai} being $\bar{B}/\sqrt{4\pi\rho_i}$.

A number of measures are taken to ensure the accuracy of the numerical results. First, a grid convergence test is made for a considerable fraction of the computations, whereby the numerical results do not show any appreciable change when the grid spacing is halved. Second, we work only with the part of the $v(a, t)$ signal when traveling disturbances have not reached r_I , meaning that the signal is not contaminated from disturbances reflected off this outer boundary. Third, we have tested other forms of the initial condition to make sure that the derived values of P and τ do not depend on this choice. However, since we are interested only in the lowest order modes, we choose not to use a too localized $v(r, t = 0)$ since this excites higher-order sausage modes as well. Fourth, for a number of $[f(r), g(r)]$, we also compute P for trapped modes by formulating Equation (1) into an eigen-value problem and then numerically solving it with a MATLAB boundary-value-problem solver BVPSUITE in its eigen-value mode (See Kitzhofer, Koch, and Weinmüller 2009 for a description of the solver, and Li *et al.* 2014 for its recent application to sausage modes). The values of P thus found agree remarkably well with those found with our initial-value-problem approach (see Figure 2).

3. Parameter study

In this section, we perform a parameter study to see how the fine structuring of a multi-shelled loop affects the period P and damping time τ of the global sausage modes. Given that $[f(r), g(r); L/a, \rho_i/\rho_e]$ constitutes too large a parameter space to exhaust, we choose to fix the density contrast ρ_i/ρ_e to be 50, in accordance with the value suggested by the event reported in Nakariakov, Melnikov, and Reznikova (2003). In addition, we fix the form of $f(r)$ to be

$$f(r) = \exp\left[-\left(\frac{r}{a}\right)^p\right], \quad p > 1. \quad (7)$$

Obviously, $\rho_{\text{mono}}(r)$ is increasingly steep when p increases. This choice of $f(r)$ is similar to the symmetric Epstein profile adopted in PNA07 when $p \approx 2$, however, a variable p also allows us to see the effects of the steepness of the monolithic density profile. Unless otherwise specified, we fix p at 2.

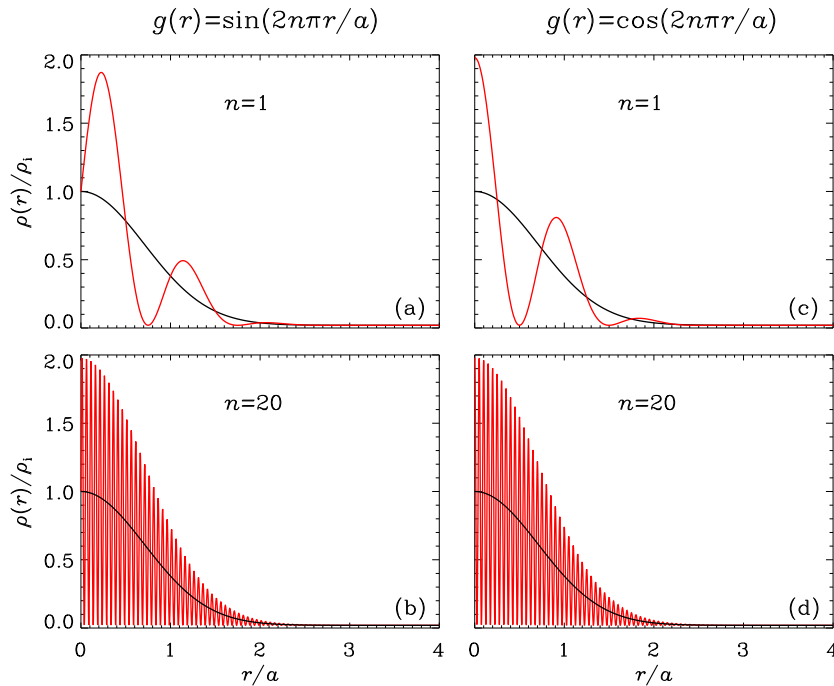


Figure 1. Equilibrium density profiles ($\bar{\rho}(r)$) with periodic fine structuring. The red curves in the left (right) column are for $\bar{\rho}(r)$ in which fine structuring is given by sinusoidal (cosinusoidal) forms. The black curves present the monolithic component, to which a modulation due to fine structuring is added. Furthermore, two values for the number of fine structures, 1 (the upper row) and 20 (lower), are adopted for illustration purposes.

3.1. Periodic Fine Structuring

Let us start with examining fine structuring of the form,

$$g(r) = \begin{cases} \sin \frac{2n\pi r}{a}, \\ \cos \frac{2n\pi r}{a}, \end{cases} \quad (8)$$

with the integer n representing the number of shells in a loop. Figure 1 shows the equilibrium density profile $\bar{\rho}$ as a function of r , with sinusoidal (cosinusoidal) modulations given by the red curves in the left (right) column. Two values of n , 1 (the upper row) and 20 (lower), are adopted for illustration purposes. For comparison, the $\bar{\rho}$ profile without fine structuring is given by the black solid lines.

Figure 2 shows the dependence on the length-to-radius ratio L/a of the period P and damping time τ . As labeled in Figure 2b, the dashed (dotted) curves correspond to the choice of $g(r)$ as a sinusoidal (cosinusoidal) function, and the red (green) curves represent the cases where $n = 1$ ($n = 100$). We note that with the asymptotic Alfvén speed v_{Ae} defined as $\bar{B}/\sqrt{4\pi\rho_e}$, the maximal period that

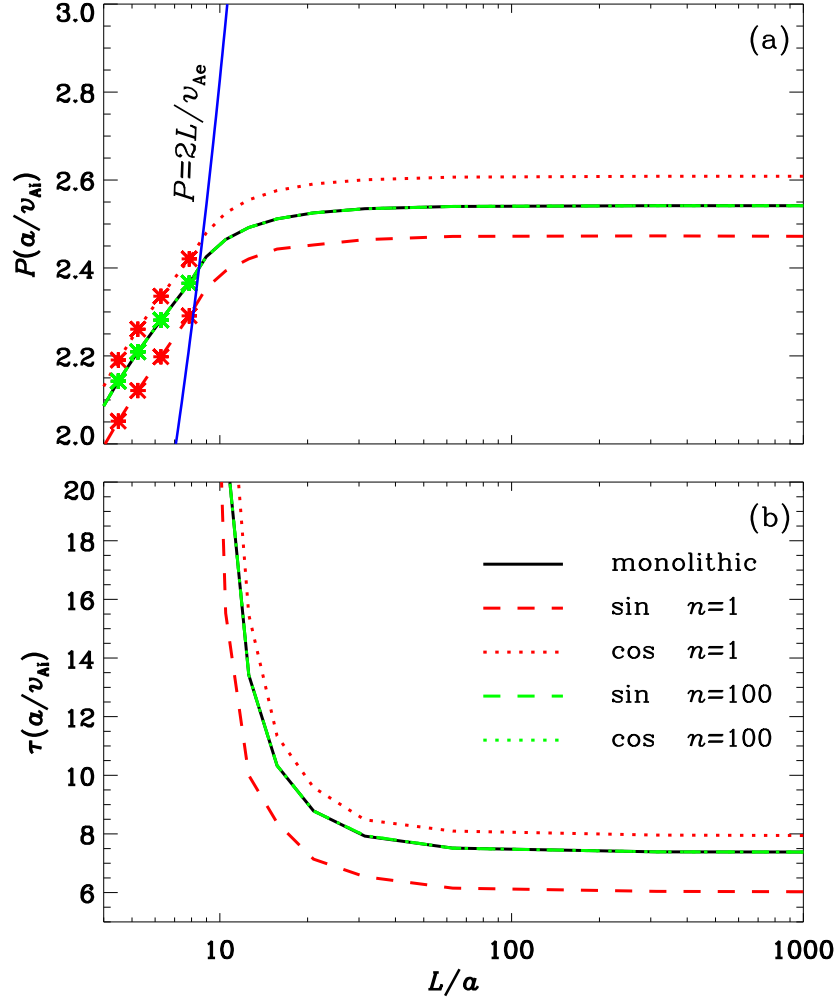


Figure 2. (a) Period P and (b) damping time τ of sausage modes supported by loops with periodic fine structuring. Here P and τ are displayed as functions of loop length L . The black curves represent the cases where fine structuring is absent. The dashed (dotted) curves are for the results where fine structuring is in a sinusoidal (cosinusoidal) form. Two values for the number of fine structures, 1 (the red curves) and 100 (green), are examined. In (a), the blue solid line separates trapped (to its left) from leaky (right) waves. Furthermore, the asterisks present the periods of trapped modes derived by solving the problem from an eigen-value-problem perspective (see text for details).

trapped modes attain is $2L/v_{Ae}$. This is given in Figure 2a by the blue solid line, which separates the trapped (to its left, where τ is identically infinite) from leaky (to its right) regimes. For comparison, the black curves represent the cases where fine structuring is absent (hardly discernible from the green curves though). The curves are found from our fitting procedure, whereas in Figure 2a the asterisks on the left of the blue line are found by formulating Equation (1) into an eigen-value problem and then solving it with BVPSUITE. Obviously, the periods P found

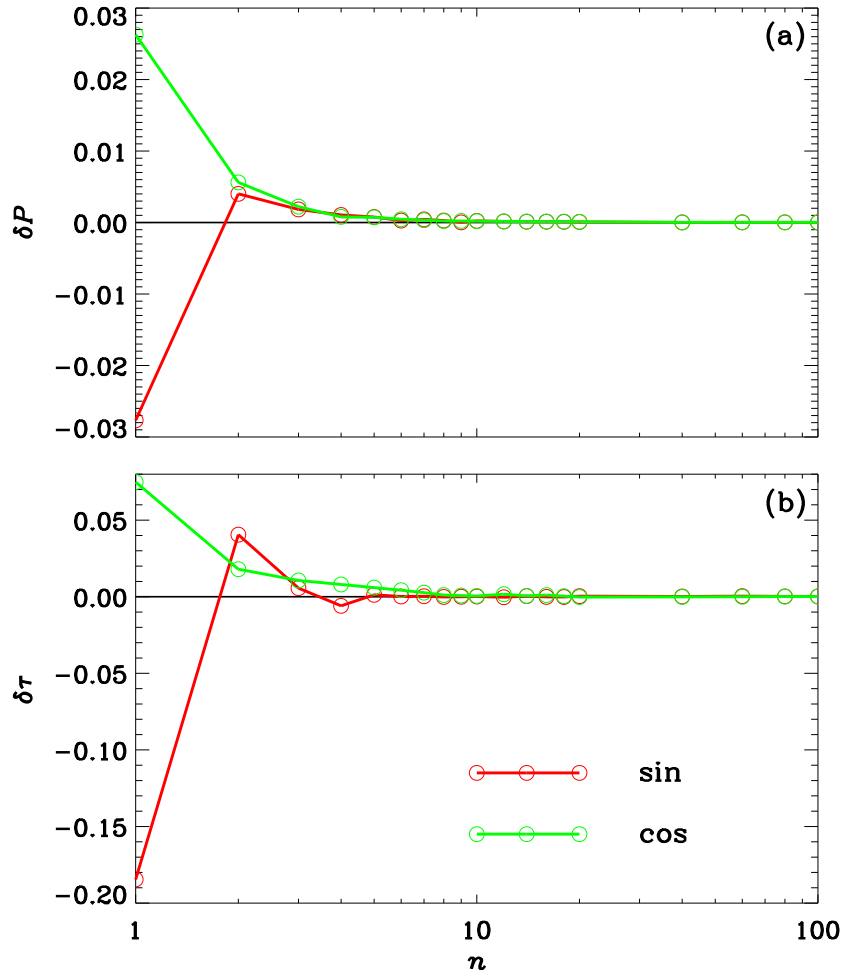


Figure 3. Dependence on the number of shells (n) of δP and $\delta\tau$, the fractional changes to the periods and damping times of sausage modes supported by thin loops with periodic fine structuring. The red (green) curves represent the cases where fine structuring is in a sinusoidal (cosinusoidal) form.

with BVPSUITE agree remarkably well with those from the fitting procedure. Figure 2 indicates that while differing in details, the overall tendency for P (τ) to increase (decrease) with L/a is seen for all the equilibrium density profiles considered. In particular, regardless of the profiles, at large values of L/a , both P and τ saturate at some asymptotic values. In addition, while for $n = 1$ (the red curves) the P and τ values show some appreciable difference from the case without fine structuring (the black curves), for $n = 100$ (the green curves) the values of P and τ can hardly be told apart from the black curves.

From the computations with the two extreme values of n ($n = 1$ and 100), one may reasonably conjecture that the larger n is, the less the effect associated with the periodic fine structuring. To see whether this is true, we employ the

fact that neither the period P nor damping time τ depends on L/a when L/a is sufficiently large. Let P_s and τ_s denote the asymptotic values that P and τ attain, respectively. The n -dependence can then be brought out by examining how varying n changes P_s and τ_s relative to the cases where fine structuring is absent (denoted by the subscript mono). These are defined as

$$\delta P \equiv \frac{P_s - P_{\text{mono},s}}{P_{\text{mono},s}}, \quad \delta \tau \equiv \frac{\tau_s - \tau_{\text{mono},s}}{\tau_{\text{mono},s}}. \quad (9)$$

Figure 3 presents (a) δP and (b) $\delta \tau$ as a function of n for $g(r)$ in the sinusoidal (cosinusoidal) form as given by the red (green) curves. One can see that indeed the fractional variations in P and τ tend to decrease in magnitude with increasing n . However, even in the cases where $n = 1$, $|\delta P|$ is no larger than 3%, and $|\delta \tau|$ remains less than 20%, with the most prominent changes found for $|\delta \tau|$ when a sinusoidal form is adopted for $g(r)$ (the red curve in Figure 3b). This happens despite that the equilibrium density profiles with fine structuring are remarkably different from the one without it (see Figures 1a and 1c). The reason for the tendency for the periodic fine structuring to have less effect with increasing number of shells is related to the transverse profile of the corresponding perturbations. While not shown here, these profiles have spatial scales of the order of the cylinder radius. With increasing n , the spatial scale ($\sim a/n$) of the transverse density profile decreases (*e.g.*, compare Figures 1a with 1b). As one expects that the effect of fine structuring maximizes when the two scales are comparable, for large values of n , the density fine structuring will have too small a transverse spatial scale to influence P or τ .

3.2. Random Fine Structuring

Compared with the periodic form, a step closer to reality will be a random distribution of the fine structures (see also PNA07). This leads us to examine

$$g(r) = \frac{R}{R_{\text{max}}}, \quad R = \sum_{n=1}^N A_n \sin\left(\frac{2n\pi r}{a} + \phi_n\right), \quad (10)$$

where A_n and ϕ_n are two independent arrays of random numbers in the ranges $[0, 1]$ and $[0, 2\pi]$, respectively. The denominator R_{max} represents the maximum that R attains, thereby ensuring that $g(r) \leq 1$. Moreover, N stands for the number of harmonics that take part in the fine structuring, and can roughly represent the number of randomly distributed concentric shells. For an illustration of the equilibrium density profile associated with such a $g(r)$, see the green curve in Figure 5b where N is set to be 60.

Obviously, with increasing N , the relative importance of the harmonics with lower n decreases. From Figure 3 we know that for single harmonics, the changes to both the period P and damping time τ decrease with increasing n . One then expects that as N increases, the influence of random fine structuring decreases. It turns out that this is indeed the case if one examines Figure 4, where the influence of fine structuring is represented by δP and $\delta \tau$, the fractional changes

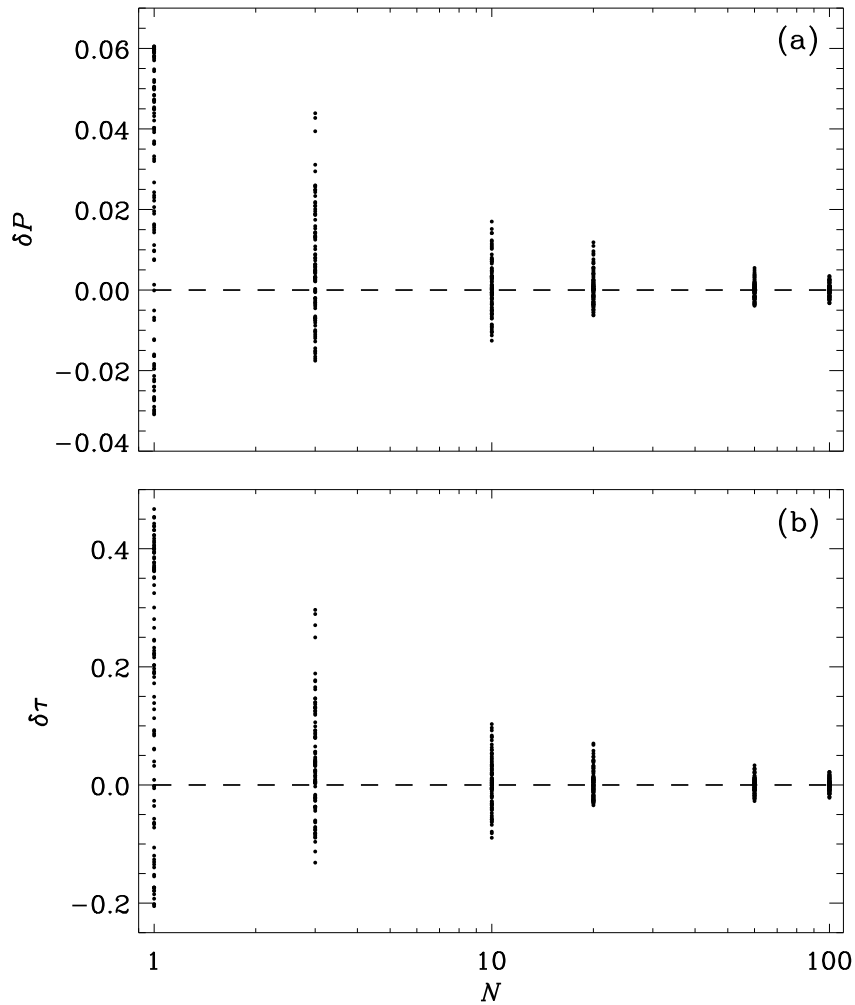


Figure 4. Dependence on N of δP and $\delta \tau$, the fractional changes to the periods and damping times of sausage modes supported by thin loops with random fine structuring. Here N represents the number of harmonics that enter into Equation (10), and can be seen as the number of randomly distributed shells. At every value of N , each dot represents one of the 100 computed realizations of the random structuring.

to the saturation values P_s and τ_s relative to the case where fine structuring is absent. Each dot for a given N represents a realization of the random function R , and in total 100 realizations are computed. Figure 4a indicates that $|\delta P|$ is consistently smaller than 6%, meaning that the period of the fundamental sausage mode is insensitive to fine structuring. Rather, it is primarily determined by the monolithic part of the equilibrium density profile. Note that this conclusion was established in PNA07 for trapped modes supported by magnetic slabs, and here we have shown that it holds for leaky modes in magnetic cylinders as well. On the other hand, Figure 4b shows that the effect due to fine structuring may be

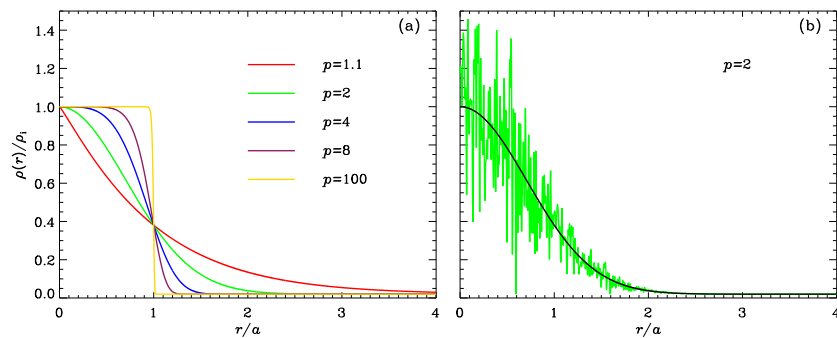


Figure 5. Equilibrium density profiles (a) without and (b) with random fine structuring. In (a), a series of values for p , the steepness parameter, is shown by curves with different colors. In (b), the black curve represents the monolithic component of the density profile given by the green curve, which includes contributions from 60 harmonics (see Equation (10)). For this monolithic component, a value of $p = 2$ is adopted.

important in determining the damping time: for some realizations $\delta\tau$ can reach 47%. However, $\delta\tau$ becomes less than 10% when $N \gtrsim 10$. Let us consider what this implies for coronal seismology, assuming that only P and τ are available as observables and as generally accepted, loops consist of a substantial number of fine structures. The negative side is that the information on fine structuring can not be probed since the changes to P and τ due to fine structuring may be well below measurement uncertainties. However, the positive side is that, when inverting the observables P and τ to infer, say, the internal Alfvén transit time, it suffices to use theoretical results accounting for only the simpler, monolithic equilibrium density profile.

3.3. Effect of the Monolithic Density Profile

So far we have fixed the steepness index p to be 2 when specifying $f(r)$. One may naturally question what would happen if p is varied? To start, let us illustrate how p influences the monolithic part of the transverse density profile as given in Figure 5a. As expected, the monolithic density profile becomes steeper as p increases.

Figure 6a shows the variation with p of P_s (the red dots) and τ_s (green), the saturation values of the period and damping time. A random structuring as given by Equation (10) with $N = 60$ is adopted. Any dot at each value of p represents one of the 100 realizations of the random function R , while the curves correspond to the case where random structuring is absent. The relative changes δP and $\delta\tau$ are then presented in Figures 6b and 6c, respectively. One can see that the effect of fine structuring tends to increase with increasing p . In fact, for $p = 1.1$, the dots in Figure 6a hardly show any appreciable deviation from the curves, a result naturally expected since Figures 6b and 6c indicate that $|\delta P|$ and $|\delta\tau|$ are no larger than 1%. In contrast, for $p = 100$, Figures 6b and 6c indicate that $|\delta P|$ and $|\delta\tau|$ may be up to 3.48% and 7.53%. However, these values at a given p are marginal to say the most when compared with the changes to P_s and τ_s due to variations in the steepness index p . For instance, Figure 6a shows that in the case

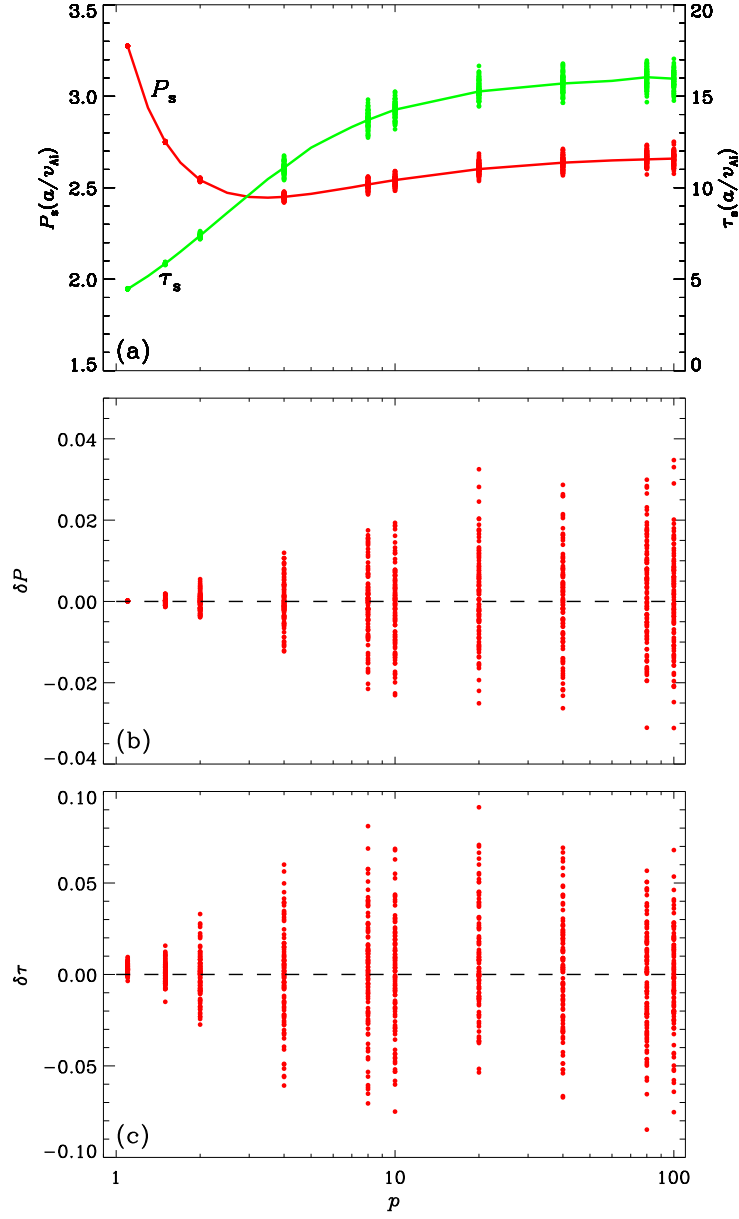


Figure 6. Dependence on p , the density profile steepness, of the periods P_s and damping times τ_s of sausage modes supported by thin loops with random fine structuring. In panel (a), the absolute values of P_s and τ_s are given, while their fractional changes relative to the cases where fine structuring is absent are given in panels (b) and (c), respectively. The random fine structuring includes 60 harmonics. For every p value, each dot represents one of the 100 realizations of the random fine structuring.

without fine structuring, τ_s increases monotonically with p , attaining $4.46 a/v_{Ai}$ ($16 a/v_{Ai}$) when $p = 1.1$ ($p = 100$). In relative terms, τ_s with $p = 100$ is 3.58 times that in the case where $p = 1.1$. From this comparison we conclude that at least for the density profiles we explored, compared with the fine structures, the monolithic part plays a far more important role in determining the period and damping time.

4. Conclusions

On both theoretical and observational grounds, magnetic loops in the solar corona are suggested to comprise a multitude of fine structures with transverse scales much shorter than loop widths. From the coronal seismology perspective, while the effects of fine structuring in the form of multilayered slabs on the periods of trapped, standing sausage modes were shown to be at most marginal (Pascoe, Nakariakov, and Arber, 2007), it remains to be seen whether the conclusion also holds for coronal cylinders and for leaky modes. Working in the framework of cold magnetohydrodynamics (MHD), we model coronal loops as magnetized cylinders with a transverse equilibrium density profile comprising a monolithic part and a modulation due to fine structuring. This kind of fine structuring can be thought of as constituting concentric shells sharing the same axis with the cylinder itself. We focused on fundamental modes with the simplest transverse structure, namely, the lowest order sausage modes without extra nodes between the two ends of the cylinder. The equation governing the transverse velocity perturbation was solved with an initial-value-problem approach, thereby the period P and damping time τ were derived by numerically fitting the signals at some given location away from the cylinder axis. Both P and τ were shown to saturate at some asymptotic values in the slender-cylinder limit. This enabled us to adopt δP and $\delta\tau$, the fractional changes to these saturation values relative to the cases where fine structuring is absent, as indicators of the effects associated with the presence of fine structuring.

Starting with an examination of periodical fine structures, we showed that as the number of shells increases, the effects on the period and damping time of leaky sausage modes decrease. This is attributed to the disparity between the characteristic transverse scale of the velocity perturbation and the increasingly small scale of the fine structures with increasing shell number. When the shell number exceeds ~ 2 , both δP and $\delta\tau$ amount to a few percent. Going a step closer to reality, we examined whether random fine structuring can have a more prominent effect in determining P and τ . While δP and $\delta\tau$ are indeed larger for some realizations of the fine structuring than in the cases with periodic structuring, when the number of fine structures (roughly represented by the number of harmonics that enter into the random structuring) exceeds ~ 10 , neither δP nor $\delta\tau$ is in excess of 10%. We showed by varying the steepness of the monolithic part of the density profile that this change may bring forth changes to P and τ by a factor of several, far more prominent than the effects due to fine structuring.

Our findings can be considered positive news for seismological applications of the period and damping time of leaky sausage modes using theoretically (*e.g.*, Kopylova *et al.*, 2007; Vasheghani Farahani *et al.*, 2014) or numerically (*e.g.*, Nakariakov, Hornsey, and Melnikov, 2012) derived P and τ where fine structuring is neglected. However, formulating fine structures as concentric shells should be considered only a preliminary step closer to reality. Fine structures in realistic coronal loops may be organized as randomly distributed strands, thereby requiring the problem be formulated as a two-dimensional one in the plane transverse to coronal cylinders (*e.g.*, Luna *et al.*, 2010). Furthermore, to simplify our treatment, we have neglected the finite plasma beta and the longitudinal variation of the equilibrium magnetic field or density. These two factors are unlikely to be important, though (see Pascoe *et al.*, 2009; Inglis *et al.*, 2009).

Acknowledgments This research is supported by the 973 program 2012CB825601, National Natural Science Foundation of China (41174154, 41274176, 41274178, and 41474149), and by the Provincial Natural Science Foundation of Shandong via Grant JQ201212.

References

- Arregui, I., Andries, J., Van Doorselaere, T., Goossens, M., Poedts, S.: 2007, MHD seismology of coronal loops using the period and damping of quasi-mode kink oscillations. *Astron. Astrophys.* **463**, 333. DOI. ADS. [2007A&A...463..333A]
- Aschwanden, M.J., Nakariakov, V.M., Melnikov, V.F.: 2004, Magnetohydrodynamic Sausage-Mode Oscillations in Coronal Loops. *Astrophys. J.* **600**, 458. DOI. ADS. [2004ApJ...600..458A]
- Brooks, D.H., Warren, H.P., Ugarte-Urra, I.: 2012, Solar Coronal Loops Resolved by Hinode and the Solar Dynamics Observatory. *Astrophys. J. Lett.* **755**, L33. DOI. ADS. [2012ApJ...755L..33B]
- Brooks, D.H., Warren, H.P., Ugarte-Urra, I., Winebarger, A.R.: 2013, High Spatial Resolution Observations of Loops in the Solar Corona. *Astrophys. J. Lett.* **772**, L19. DOI. ADS. [2013ApJ...772L..19B]
- Chen, S.-X., Li, B., Xia, L.-D., Chen, Y.-J., Yu, H.: 2014, Effects of Field-Aligned Flows on Standing Kink and Sausage Modes Supported by Coronal Loops. *Solar Phys.* **289**, 1663. DOI. ADS. [2014SoPh...289.1663C]
- Chen, Y., Song, H.Q., Li, B., Xia, L.D., Wu, Z., Fu, H., Li, X.: 2010, Streamer Waves Driven by Coronal Mass Ejections. *Astrophys. J.* **714**, 644. DOI. ADS. [2010ApJ...714..644C]
- Chen, Y., Feng, S.W., Li, B., Song, H.Q., Xia, L.D., Kong, X.L., Li, X.: 2011, A Coronal Seismological Study with Streamer Waves. *Astrophys. J.* **728**, 147. DOI. ADS. [2011ApJ...728..147C]
- Goossens, M., Erdélyi, R., Ruderman, M.S.: 2011, Resonant MHD Waves in the Solar Atmosphere. *Space Sci. Rev.* **158**, 289. DOI. ADS. [2011SSRv...158..289G]
- Goossens, M., Arregui, I., Ballester, J.L., Wang, T.J.: 2008, Analytic approximate seismology of transversely oscillating coronal loops. *Astron. Astrophys.* **484**, 851. DOI. ADS. [2008A&A...484..851G]
- Guarrasi, M., Reale, F., Peres, G.: 2010, Coronal Fuzziness Modeled with Pulse-heated Multi-stranded Loop Systems. *Astrophys. J.* **719**, 576. DOI. ADS. [2010ApJ...719..576G]
- Heyvaerts, J., Priest, E.R.: 1983, Coronal heating by phase-mixed shear Alfvén waves. *Astron. Astrophys.* **117**, 220. ADS. [1983A&A...117..220H]
- Hornsey, C., Nakariakov, V.M., Fludra, A.: 2014, Sausage oscillations of coronal plasma slabs. *Astron. Astrophys.* **567**, A24. DOI. ADS. [2014A&A...567A..24H]
- Inglis, A.R., van Doorselaere, T., Brady, C.S., Nakariakov, V.M.: 2009, Characteristics of magnetoacoustic sausage modes. *Astron. Astrophys.* **503**, 569. DOI. ADS. [2009A&A...503..569I]

- Kitzhofer, G., Koch, O., Weinmüller, E.: 2009, Numerical Treatment of Singular BVPs: The New MATLAB Code bvpsuite. In: Simos, T.E., Psihoyios, G., Tsitouras, C. (eds.) *American Institute of Physics Conference Series, American Institute of Physics Conference Series* **1168**, 39. DOI. ADS. [2009AIPC.1168...39K]
- Kopylova, Y.G., Melnikov, A.V., Stepanov, A.V., Tsap, Y.T., Goldvarg, T.B.: 2007, Oscillations of coronal loops and second pulsations of solar radio emission. *Astronomy Letters* **33**, 706. DOI. ADS. [2007AstL...33..706K]
- Li, B., Habbal, S.R., Chen, Y.: 2013, The Period Ratio for Standing Kink and Sausage Modes in Solar Structures with Siphon Flow. I. Magnetized Slabs. *Astrophys. J.* **767**, 169. DOI. ADS. [2013ApJ...767..169L]
- Li, B., Chen, S.-X., Xia, L.-D., Yu, H.: 2014, Standing sausage modes in coronal loops with plasma flow. *Astron. Astrophys.* **568**, A31. DOI. ADS. [2014A&A...568A..31L]
- Luna, M., Terradas, J., Oliver, R., Ballester, J.L.: 2010, Transverse Oscillations of a Multi-stranded Loop. *Astrophys. J.* **716**, 1371. DOI. ADS. [2010ApJ...716.1371L]
- Murawski, K., Nakariakov, V.M., Pelinovsky, E.N.: 2001, Fast magnetoacoustic waves in a randomly structured solar corona. *Astron. Astrophys.* **366**, 306. DOI. ADS. [2001A&A...366..306M]
- Nakariakov, V.M., Melnikov, V.F.: 2009, Quasi-Periodic Pulsations in Solar Flares. *Space Sci. Rev.* **149**, 119. DOI. ADS. [2009SSRv...149..119N]
- Nakariakov, V.M., Ofman, L.: 2001, Determination of the coronal magnetic field by coronal loop oscillations. *Astron. Astrophys.* **372**, L53. DOI. ADS. [2001A&A...372L..53N]
- Nakariakov, V.M., Verwichte, E.: 2005, Coronal Waves and Oscillations. *Living Reviews in Solar Physics* **2**, 3. DOI. ADS. [2005LRSP....2....3N]
- Nakariakov, V.M., Hornsey, C., Melnikov, V.F.: 2012, Sausage Oscillations of Coronal Plasma Structures. *Astrophys. J.* **761**, 134. DOI. ADS. [2012ApJ...761..134N]
- Nakariakov, V.M., Melnikov, V.F., Reznikova, V.E.: 2003, Global sausage modes of coronal loops. *Astron. Astrophys.* **412**, L7. DOI. ADS. [2003A&A...412L..7N]
- Pascoe, D.J., Nakariakov, V.M., Arber, T.D.: 2007, Sausage Oscillations in Multishell Coronal Structures. *Solar Phys.* **246**, 165. DOI. ADS. [2007SoPh..246..165P]
- Pascoe, D.J., Nakariakov, V.M., Arber, T.D., Murawski, K.: 2009, Sausage oscillations in loops with a non-uniform cross-section. *Astron. Astrophys.* **494**, 1119. DOI. ADS. [2009A&A...494.1119P]
- Peter, H., Bingert, S., Klimchuk, J.A., de Forest, C., Cirtain, J.W., Golub, L., Winebarger, A.R., Kobayashi, K., Korreck, K.E.: 2013, Structure of solar coronal loops: from miniature to large-scale. *Astron. Astrophys.* **556**, A104. DOI. ADS. [2013A&A...556A.104P]
- Reale, F., Peres, G.: 2000, TRACE-derived Temperature and Emission Measure Profiles along Long-lived Coronal Loops: The Role of Filamentation. *Astrophys. J. Lett.* **528**, L45. DOI. ADS. [2000ApJ...528L..45R]
- Roberts, B., Edwin, P.M., Benz, A.O.: 1984, On coronal oscillations. *Astrophys. J.* **279**, 857. DOI. ADS. [1984ApJ...279..857R]
- Stepanov, A.V., Zaitsev, V.V., Nakariakov, V.M.: 2012, *Stellar Coronal Seismology as a Diagnostic Tool for Flare Plasma*. DOI. ADS. [2012scsd.book.....S]
- Tripathi, D., Mason, H.E., Dwivedi, B.N., del Zanna, G., Young, P.R.: 2009, Active Region Loops: Hinode/Extreme-Ultraviolet Imaging Spectrometer Observations. *Astrophys. J.* **694**, 1256. DOI. ADS. [2009ApJ...694.1256T]
- Van Doorselaere, T., Brady, C.S., Verwichte, E., Nakariakov, V.M.: 2008, Seismological demonstration of perpendicular density structuring in the solar corona. *Astron. Astrophys.* **491**, L9. DOI. ADS. [2008A&A...491L..9V]
- Vasheghani Farahani, S., Hornsey, C., Van Doorselaere, T., Goossens, M.: 2014, Frequency and Damping Rate of Fast Sausage Waves. *Astrophys. J.* **781**, 92. DOI. ADS. [2014ApJ...781...92V]
- Warren, H.P., Winebarger, A.R., Mariska, J.T.: 2003, Evolving Active Region Loops Observed with the Transition Region and Coronal explorer. II. Time-dependent Hydrodynamic Simulations. *Astrophys. J.* **593**, 1174. DOI. ADS. [2003ApJ...593.1174W]
- Warren, H.P., Ugarte-Urra, I., Doschek, G.A., Brooks, D.H., Williams, D.R.: 2008, Observations of Active Region Loops with the EUV Imaging Spectrometer on Hinode. *Astrophys. J. Lett.* **686**, L131. DOI. ADS. [2008ApJ...686L.131W]
- Yuan, D., Pascoe, D.J., Nakariakov, V.M., Li, B., Keppens, R.: 2015, Evolution of Fast Magnetoacoustic Pulses in Randomly Structured Coronal Plasmas. *Astrophys. J.* **799**, 221. DOI. ADS. [2015ApJ...799..221Y]